Clay Minerals (2023), **58**, 335–344
doi:10.1180/clm.2023.30

CAMBRIDGE UNIVERSITY PRESS

Article

The implications of Fe speciation for the humic substance stability of ternary Fe(III)–montmorillonite–humic substance systems

Qinkai Lei[1,2,†], Yahui Lv[2,†], Chengshuai Liu[3], Wenpo Xu[2], Shujie Hu[2], Manjia Chen[2], Hongling Bu[1,2] and Junhui Li[1]

[1]School of Environmental Science and Engineering, Guangdong University of Technology, Guangzhou, China; [2]National–Regional Joint Engineering Research Center for Soil Pollution Control and Remediation in South China, Guangdong Key Laboratory of Integrated Agro-environmental Pollution Control and Management, Institute of Eco-environmental and Soil Sciences, Guangdong Academy of Sciences, Guangzhou, China and [3]State Key Laboratory of Environmental Geochemistry, Institute of Geochemistry, Chinese Academy of Sciences, Guiyang, China

Abstract

Mineral–organic matter (OM) associations play an important role in determining the long-term retention of OM in soils. However, the retention mechanisms of OM in cation–mineral–OM systems remain unclear. Taking into account the dominance of montmorillonite (Mnt) in the soil of the temperate zone, we investigated the stability of humic substances (HSs) in the Fe(III)–Mnt–HS system using thermal analysis. The HS degradation started at ~387°C in the Fe(III)–Mnt–HS system, which was higher than that of the Fe(III)–HS system (290°C). The formed ferrihydrite (Fhy) mainly contributed to the enhanced labile OM retention through adsorption and/or co-precipitation, whereas Mnt inhibited the initial formation and subsequent transformation of Fhy, thus improving the stability of OM. These results suggest that the HS stability in Fe(III)–clay–HS systems depends on the Fe speciation affected by clay minerals, and this finding provides insights into OM–mineral interactions in temperate-zone soils.

Keywords: Fe speciation, humic substances, mineral–organic association, montmorillonite, thermal analysis

(Received 27 March 2023; revised 10 October 2023; Accepted Manuscript online: 6 November 2023; Guest Editor: Hongjuan Sun)

Soil organic matter (SOM) represents the largest reservoir of terrestrial carbon (C) worldwide and is an important component of the C source in all terrestrial ecosystems. SOM is a complex mixture of polyelectrolytes produced by the biotic and abiotic alteration/degradation of organic compounds of plant and animal origin (Paul, 2016). Thus, SOM consists of organic compounds with different chemical structures, and it forms *via* distinct pathways depending on whether the inputs that are water soluble and/or are easily solubilized enter the soil, such as dissolved OM, mineral-associated OM and particulate OM (Cotrufo *et al.*, 2022). Therefore, SOM persistence could be a function of biotic and abiotic processes in the soil, such as climate and soil geochemical characteristics (i.e. microbial activity and association of minerals).

Minerals are among the primary soil parameters that determine SOM persistence (Kleber *et al.*, 2015). In soils and sediments, a variety of minerals are present. These soil minerals are dominated by the clay fraction (<2 μm), which is a mixture of phyllosilicate clay minerals, aluminium (Al) and iron (Fe) oxides, oxyhydroxides and hydroxides (together known as oxides). Phyllosilicate clay minerals are the primary components in most soils (Cotrufo *et al.*, 2022). These soil components could preserve SOM through the formation of mineral–OM associations (MOAs; Mikutta *et al.*, 2006; Chen *et al.*, 2014; Kleber *et al.*, 2015), which are an essential form of stable OM (Parfitt *et al.*, 1997; Barré *et al.*, 2014; Kopittke *et al.*, 2020). As a result, several research studies have focused on the role of soil minerals in the persistence of SOM.

Soil clay minerals influence the stabilization of soil humus through accumulating humic monomers, catalysing the abiotic polymerization of the adsorbed humic monomers and physically sequestering some OM and hence making OM unavailable to soil microorganisms (Bosetto *et al.*, 1997; Ahmat *et al.*, 2019; Bu *et al.*, 2019). The adsorption sites of clay minerals, such as montmorillonite (Mnt) and kaolinite, are mainly silicon hydroxyl (Si-OH) and aluminium hydroxyl (Al-OH) sites, which can interact with OM with deprotonated functional groups (e.g. carboxyl and phenolic hydroxyl) through a cation bridge and/or hydrogen bonding (Lützow *et al.*, 2006). Research has shown that clay minerals with more swelling layers might contribute to the retention of OM and improve carbon stabilization in soil (Barré *et al.*, 2014). In addition, metal oxides could accumulate OM *via* a surface complexation reaction at an iron hydroxyl (Fe-OH) site and have greater sorption potential than phyllosilicates (Tombácz *et al.*, 2004; Chen *et al.*, 2014). Some studies have concluded that the abundance and stocks of organic carbon (OC) typically increase as both clay and Fe/Al oxide contents increase in tropical ecosystems and beyond (Bruun *et al.*, 2010).

In addition to these inorganic minerals, multivalent cations (i.e. Fe^{3+} and Al^{3+}) are frequently present in soils with concentrations up to hundreds of micromolar (Yang *et al.*, 2017). By binding minerals and OM, these cations might enhance the retention of OC on mineral surfaces and decrease the desorption of soluble OM from soils (Muneer & Oades, 1989; Hobbie *et al.*, 2007).

†These authors contributed equally to this work.

Corresponding author: Hongling Bu; Email: buhongling@gdut.edu.cn

This paper was submitted for the special issue devoted to ICC2022.

Cite this article: Lei Q, Lv Y, Liu C, Xu W, Hu S, Chen M, Bu H, Li J (2023). The implications of Fe speciation for the humic substance stability of ternary Fe(III)–montmorillonite–humic substance systems. *Clay Minerals* **58**, 335–344. https://doi.org/10.1180/clm.2023.30

Moreover, they might contribute to improving OM retention *via* Fe (III)–OM precipitation (Chen *et al.*, 2014) or Fe (hydr) oxide-induced adsorption and co-precipitation in OM-containing solution systems (Chen *et al.*, 2014). Furthermore, previous studies have demonstrated that MOAs are held together by these cations (Muneer & Oades, 1989), especially in smectitic soils (Wattel-Koekkoek *et al.*, 2001). These findings suggest that the presence of Ca^{2+}, especially in Mnt soils, could favour the formation of larger C soil reservoirs (Sutton & Sposito, 2006). However, in addition to Ca^{2+}, ternary systems that include Fe^{3+}, minerals and OM are widespread in the soil. Previous studies have suggested that the hydrolysis of Fe^{3+} in solution could form Fe (hydr)oxide, while the presence of OM or inorganic minerals might be suppressed (Karlsson & Persson, 2012; Meng *et al.*, 2022). Consequently, the presence of Fe^{3+} could affect the persistence of SOM because hydrolysis, Fe^{3+}precipitation and subsequent ageing would restrict Fe(III)–mineral–OM interactions.

Humic substances (HSs) are organic compounds that naturally occur during long-term decomposition of biomass residue, constituting some of the greatest components of SOM and some of the most common OM present in soil solutions. Notably, the organic components might be dissolved as discrete particles in the soil or coatings on the surface of minerals (Schnitzer & Monreal, 2011). Mnt, as a member of the smectite group, is a 2:1 clay mineral with a central octahedral sheet of alumina sandwiched between two tetrahedral sheets of silica, and it is commonly found in a variety of soils in the temperate zone (Kleber *et al.*, 2015). The swelling of Mnt in aqueous solutions enables the intercalation of OM and greatly retards the microbial mineralization of SOM. However, the stabilization of HSs during the reaction between co-precipitated Fe(III) and Mnt remains unclear. Hence, it is necessary to acquire basic knowledge regarding the persistence and functioning of HSs in Fe(III)–clay-based temperate-zone soils in order to comprehend the significance of mineral matrices for HSs.

In this study, we investigated the effects of co-precipitated HSs on the Fe(III)–Mnt–HS system and discussed the persistence of HSs. Specifically, the stability of OM was evaluated by testing its susceptibility to decomposition during pyrolysis under an N_2 atmosphere. Thermal analysis (i.e. thermal gravimetric analysis (TGA) and differential scanning calorimetry (DSC)) is vital tool for investigating the thermal evolution of SOM (Lopez-Capel *et al.*, 2005; Plante *et al.*, 2005; Tokarski *et al.*, 2020). Thermal analysis provides information on the energy input required to break down organic molecules during combustion and the energy yield associated with this breakdown, whether consumed or released (Peltre *et al.*, 2013). These parameters of HS stability are then compared across mineral types to assess how clay-sized Al phases and Fe oxides influence OM stability. The results of this study provide insights into the influence of cation–mineral–OM systems on OC stabilization.

Experimental

Materials

The Mnt SAz-2 was obtained from the Clay Minerals Society. The as-received chunky sample was ground to a powder before being used in this study. After purification and Ca saturation, the Mnt product was obtained. The HSs were purchased from Aladdin Industrial Corporation (CAS No. 1415-93-6). The composition was >90% fulvic acid and was used directly without further purification. Solution HSs were prepared *via* the dissolution of HSs in 0.1 mol L^{-1} NaOH. The Fe (hydr)oxide was prepared as described in Schwertmann & Cornell (2008). For Fe(III)–mineral–OM systems, Fe (hydr)oxide solutions were co-precipitated with Mnt–HS solutions. Specifically, 2.7 g of $FeCl_3{\cdot}6H_2O$ was added to 50 mL Milli-Q water (18.2 MΩ) in the presence of HS or Mnt–HS solutions. The weight ratio of Fe/Mnt was 2:1 and the HS concentration was 10%. NaOH solution at a concentration of 1 mol L^{-1} was slowly added until the pH reached 7.0. Then, the turbid solution was aged at room temperature for 4 h. At that point, the pH decreased slightly, and the pH was reset to 7.0. The turbid liquid was centrifuged at 10 000 rpm for 15 min. The supernatant was discarded and the products were washed with Milli-Q water four times to remove excess Cl^-. Subsequently, the solids were freeze-dried, ground with a pestle and mortar and placed in anoxic gloveboxes. The products were denoted as Fe(III)–Mnt–HS, Fe(III)–HS and Mnt–HS, respectively. For the control treatment, Fe (hydr)oxide and Mnt solutions were co-precipitated with HS solutions to prepare Fe(III)–OM and Mnt–OM MOAs, respectively.

Characterization

A Thermo FLASH2000 element analysis instrument was utilized to measure the total OC content in the samples. X-ray photoelectron spectroscopy (XPS) was applied to study the surface elemental composition of the samples. The XPS spectra were collected with a Thermo Scientific K-Alpha XPS device with an Al-K X-ray source. The charge effect was corrected by adjusting the binding energy of C 1s to 284.8 eV. The C and O spectra were fitted using the *Avantage* software with the peaks of the Gaussian–Lorentzian mixed function.

The mineralogy of the samples was confirmed on freeze-dried subsamples *via* X-ray diffraction (XRD). Powder XRD analysis was performed using a Bruker D2 PHASER diffractometer with a copper source (λ = 0.154 nm, 30 kV and 30 mA). The samples were collected from 8° to 80° at a scanning rate of 1°2θ min^{-1}, and the Mnt-based samples were scanned from 3 to 80°2θ to verify possible intercalations. The data were collected using a 12 mm divergence slit, a 12 mm filament length, a 15 mm sample length and 2.5° Soller slits. A Thermo Scientific Nicolet iS20 infrared spectrometer was used to perform Fourier-transform infrared (FTIR) spectroscopy characterization. The spectral collection range was 400–4000 cm^{-1}. The spectra represent the average of 32 scans at a resolution of 4 cm^{-1}.

The thermal stability of the samples was studied using TGA and DSC with a Netzsch STA-2500 thermal analyser under an inert N_2 atmosphere. Before the experiment, the samples were sieved through a 100 mesh sieve before being tested and then weighed (~10 mg) and placed in an open alumina crucible. A heating rate of 5°C min^{-1} was used to heat the samples from 30°C to 800°C.

After preparation and characterization of the MOAs, heat ageing tests of the MOAs in an anaerobic environment were conducted. The solids were weighed into porcelain boats and heated at 200°C, 300°C and 400°C under a steady flow of N_2 at a heating rate of 10°C min^{-1}. The heating rate was maintained constant for 3 h. At each sampling, the solids were collected after cooling to room temperature and analysed at pre-designated times to monitor the changes in the physicochemical characteristics of the MOAs. The temperatures used in the ageing experiments were specifically chosen as they revealed the greatest variation in

https://doi.org/10.1180/clm.2023.30 Published online by Cambridge University Press

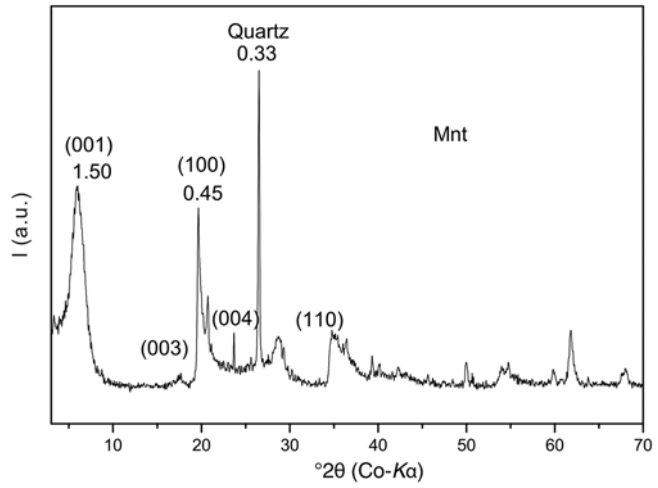

Figure 1. XRD trace of Mnt. Labels represent *d*-spacing values in nanometres.

mass during thermal degradation compared to those observed during TGA.

Results

Properties of MOAs

The XRD trace of Mnt is illustrated in Fig. 1. The basal spacing of Mnt was 1.50 nm. The XRD traces of the MOAs show a 2.58 Å ferrihydrite (Fhy) peak (Fig. 2), suggesting that amorphous two-line Fhy is the main Fe phase. Other broad peaks in the XRD trace of Fe(III)–HS were also identified, corresponding to the OM or other inorganic minerals from the co-precipitated HSs. For Mnt–HS, a d_{001} spacing of 1.40 nm was observed, which indicates intercalation of organic molecules in the interlayer space of Mnt. This observation is consistent with the previous finding that some humic acid molecules can be partially incorporated into the interlayer space of Mnt (Ye *et al.*, 2022). However, for Fe(III)–Mnt–HS, the introduction of Fe shifted the (001) peak to a lower *d*-spacing (1.25 nm for Fe(III)–Mnt–HS and 1.50 nm for Mnt), suggesting that some Fe ions or some organic molecules entered the interlayer *via* exchange with Ca^{2+} (Fig. 1 & inset of Fig. 2).

The elemental compositions of the HSs and MOAs are shown in Table 1. The C content ranges from 5.17% to 41.83%, while the N and H contents vary from 0% to 0.84% and from 1.98% to 3.35%, respectively. The high C/N ratio and low H/C ratio for the HSs indicated high stability and condensation degree as well as an extended degree of humification (Rosell *et al.*, 1989). Hence, the HSs seem to be affected by the co-precipitation process, which influences their stability and degree of condensation. The low N content of the MOAs indicates that Fhy formed during co-precipitation and Mnt had separated some nitrogen-containing functional groups, whereas the high H/C ratio could be due to the addition of these minerals.

The surface elemental components were determined using XPS analysis (Figs 3 & 4 & Tables 2 & S1). Figures 3 & 4 show the high-resolution XPS spectra of C 1s and O 1s, respectively. The three main peaks at ~284.8, ~286.4 and ~288.7 eV were assigned to C–C, C–O–C and O–C=O, respectively (Zeng *et al.*, 2020). The presence of C highlights the adsorption of certain organic compounds by the samples during the co-precipitation process. Compared with the HSs alone, the proportion of C–C groups in Fe(III)–HS and Mnt–HS increased, whereas the proportion of O–C=O groups decreased. In the case of Fe(III)–Mnt–HS, the proportion of C–C groups decreased, whereas the proportion of C–O–C groups increased. The surface C changes observed after the involvement of Fhy demonstrated that these might occur either if the OM combined with Fe included the inclusion, occlusion and entrance of Fe (hydr)oxide crystals (Kleber *et al.*, 2015; Sodano *et al.*, 2017; Bao *et al.*, 2022) or if some small, fractionated OM molecules entered the interlayer space of Mnt during the co-precipitation process (Bu *et al.*, 2017).

Regarding the O 1s spectrum (Fig. 4), the fitted XPS spectrum of the HSs featured three distinct peaks at ~531.9, ~533.5 and 535.7 eV, corresponding to organic C–O, C–O–C and O–H groups, respectively. The new peak at ~530 eV for Fe(III)–HS, Mnt–HS and Fe(III)–Mnt–HS suggests the presence of metal–oxygen bonds, which is in agreement with the presence of minerals such as Fhy (Ye *et al.*, 2020). The content of C–O groups

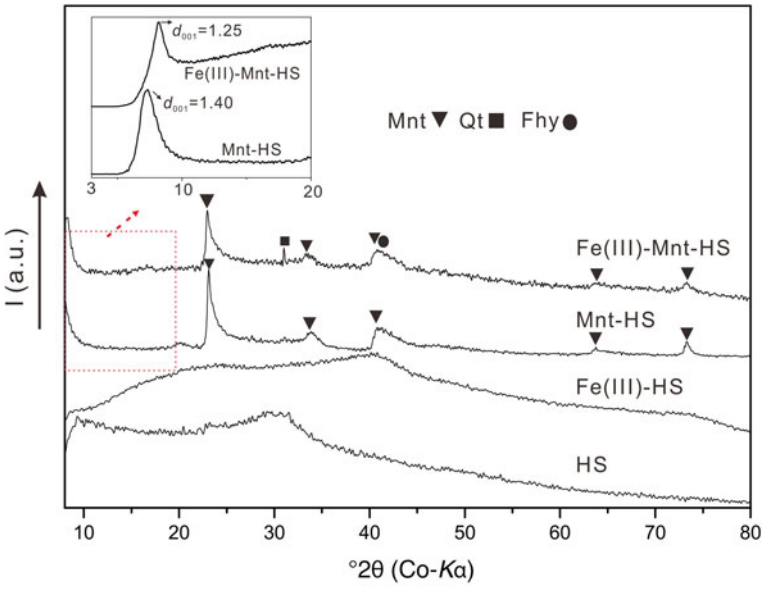

Figure 2. XRD traces of HS and the synthesized Fe(III)–HS, Mnt–HS and Fe(III)–Mnt–HS systems. Labels represent *d*-spacing values in nanometres. Qt = quartz.

https://doi.org/10.1180/clm.2023.30 Published online by Cambridge University Press

Table 1. Elemental compositions of HSs and MOAs.

Sample	C (%)	N (%)	H (%)	S (%)	C/N	H/C
HS	41.83	0.84	3.35	0.24	49.80	0.08
Fe(III)–HS	9.84	0.02	2.15	0.05	492.00	0.21
Mnt–HS	6.63	0.00	2.44	0.06	–	0.37
Fe(III)–Mnt–HS	5.17	0.00	1.98	0.03	–	0.38

decreased significantly for the Fe(III)–HS system (the atomic contents decreased significantly from 72.66% to ~26.07%) and increased for the Mnt–HS and Fe(III)–Mnt–HS systems (Table 2). Due to the Fhy and Mnt involved, the content of hydroxyl groups was significantly reduced for all the samples. The absence of C–O–C groups in the Mnt–HS and Fe(III)–Mnt–HS systems implies that the ether functional groups were diminished. This suggests that the reaction was mediated by hydroxyl-containing functional groups and/or ether linkages during the co-precipitation process. In addition, strong Fe signals were detected in both the Fe(III)–HS and Fe(III)–Mnt–HS systems. In Fe(III)–HS, total P and Fe were enriched, whereas total O, Si and Al were enriched in the Fe(III)–Mnt–HS system. In the case of Mnt–HS, the total C and N contents were lower than those of Fe(III)–HS and Fe(III)–Mnt–HS (Table S1). Accordingly, the surface fixation ability of Mnt to OC seems weaker than that of Fe(III) during the co-precipitation process. This suggests that the Fhy and Mnt act as a chromatographic system during the co-precipitation of Fe(III), and the co-precipitation of OM results in the fractionation of the compounds according to their sorption selectivity.

TGA and DSC analysis of the MOAs

The TGA data showed that the breakdown of HSs begins at >200°C (Fig. 5a). The major thermal event of pure HSs occurred between 200°C and 550°C, resulting in a sharp deriative TGA (dTGA) peak at 339°C (Fig. 5b & Table 3). The decomposition of OM with a low degree of humification was responsible for this decarboxylation. Higher temperatures of >400°C induced

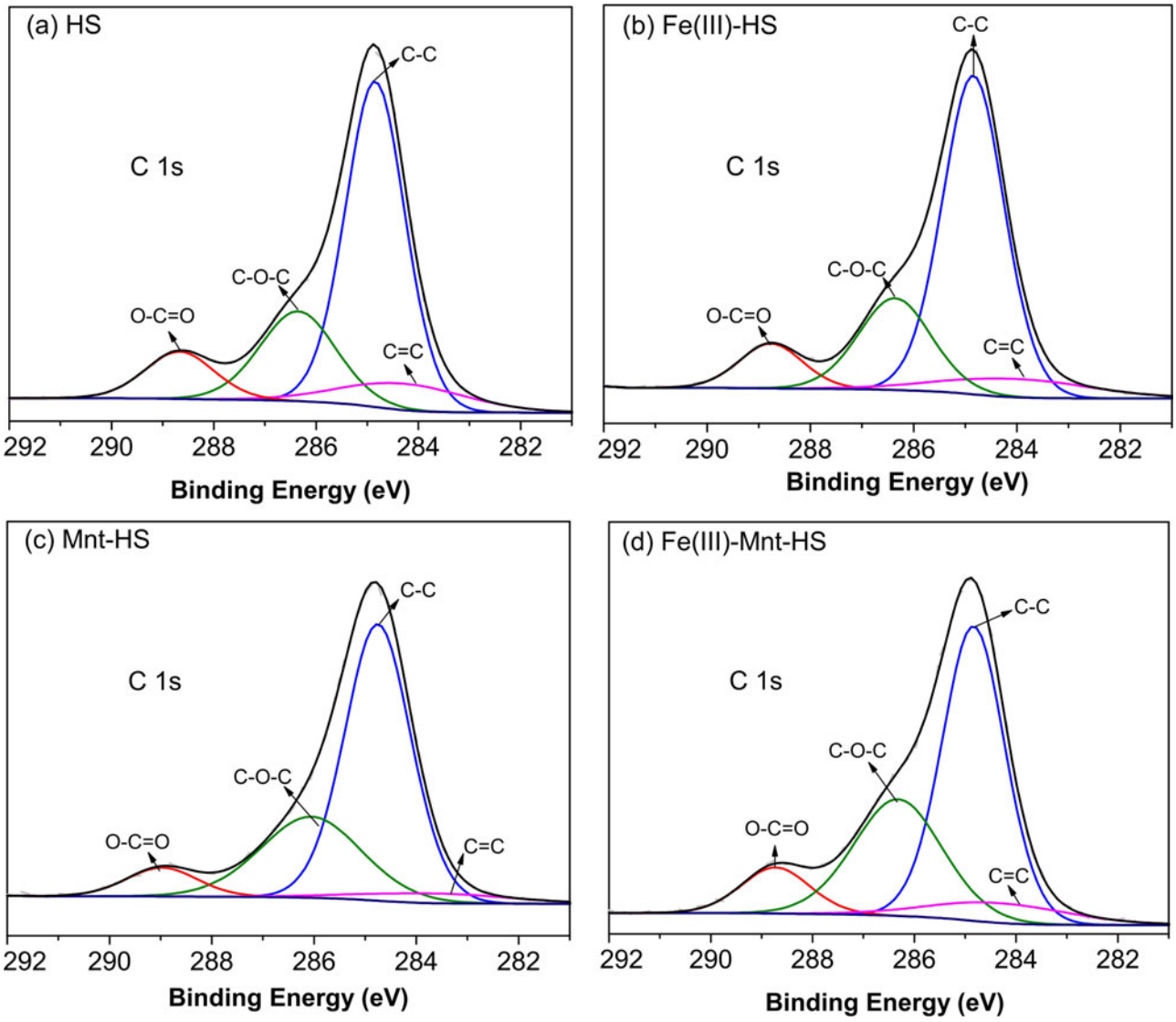

Figure 3. The C 1s XPS spectra of (a) HS, (b) Fe(III)–HS, (c) Mnt–HS and (d) Fe(III)–Mnt–HS. The grey dotted lines denote the measured XPS spectra. The black lines denote the smoothed XPS spectra.

https://doi.org/10.1180/clm.2023.30 Published online by Cambridge University Press

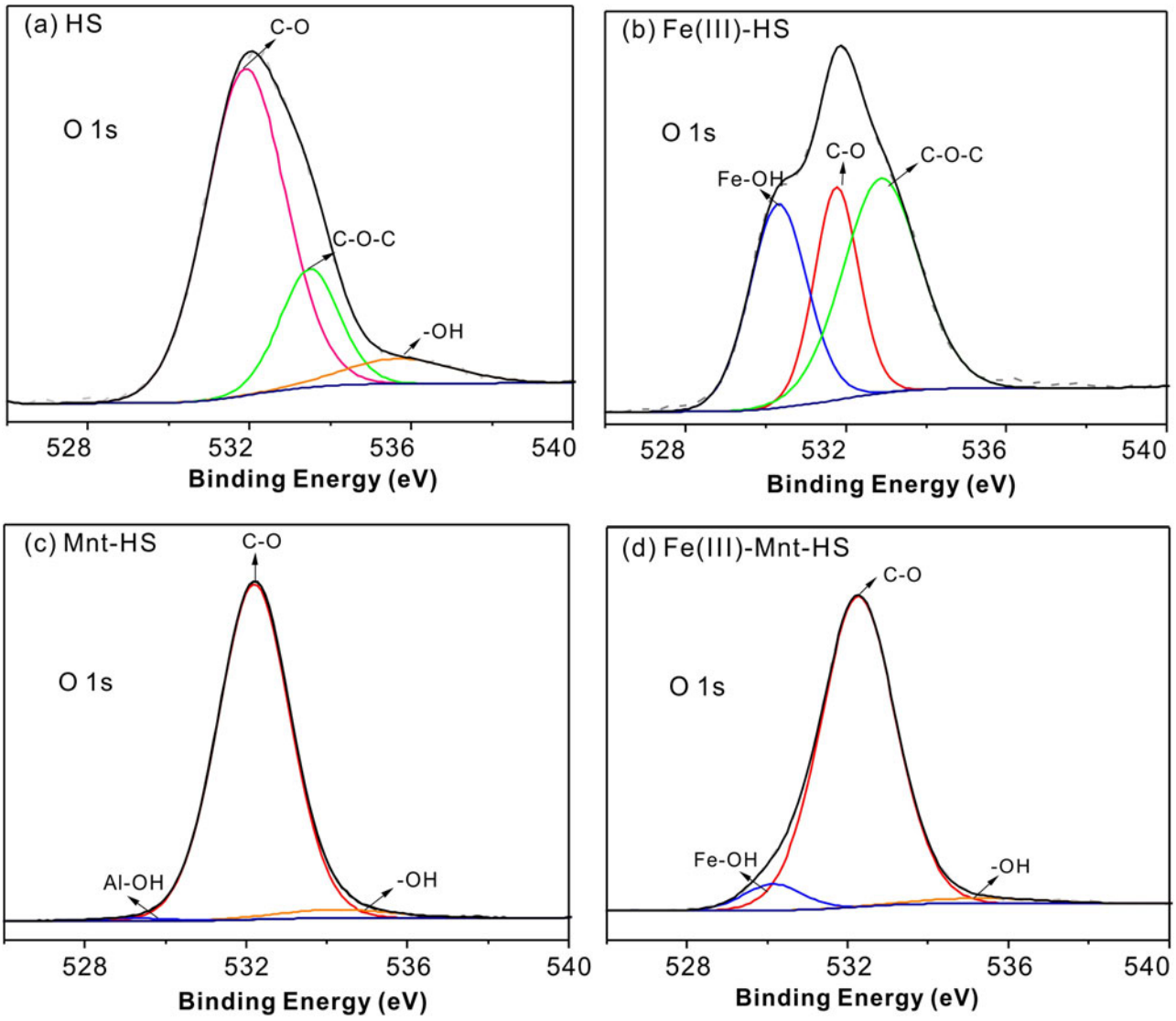

Figure 4. The O 1s XPS spectra of (a) HS, (b) Fe(III)–HS, (c) Mnt–HS and (d) Fe(III)–Mnt–HS. The grey dotted lines denote the measured XPS spectra. The black lines denote the smoothed XPS spectra.

Table 2. Analysis of C 1s and O 1s XPS spectra.

Sample	Binding energy C 1s (eV)	Chemical state	Atomic %	Binding energy O 1s (eV)	Chemical state	Atomic %
HS	284.8	C–C	59.18	531.9	C–O	72.66
	286.4	C–O–C	20.89	533.5	C–O–C	19.68
	288.7	O–C=O	9.99	535.7	–OH	7.66
	284.3	C=C	9.94			
Fe(III)–HS	284.8	C–C	61.34	531.8	C–O	26.07
	286.4	C–O–C	21.01	530.3	Fe–OH	31.08
	288.8	O–C=O	8.93	532.9	C–O–C	42.86
	284.1	C=C	8.73			
Mnt–HS	284.8	C–C	61.11	532.2	C–O	95.23
	286.1	C–O–C	27.37	534.2	–OH	3.92
	289.0	O–C=O	6.81	529.2	Al–OH	0.84
	283.6	C=C	4.72			
Fe(III)–Mnt–HS	284.8	C–C	53.26	532.2	C–O	91.33
	286.3	C–O–C	29.80	530.1	Fe–OH	6.10
	288.7	O–C=O	9.14	535.2	–OH	2.58
	284.3	C=C	7.79			

structural changes in HS macromolecules, mainly dearomatization of the ring (Barros *et al.*, 2011). The two contrasting peaks reflected by the dTGA curves were examined to divide the thermal oxidation/combustion resistance levels into two distinct categories (Demyan *et al.*, 2013; Merino & Nevado, 2014; Kurganova *et al.*, 2019; Barreto *et al.*, 2021): (1) 200–400°C (labile OM) and (2) 400–550°C (recalcitrant OM). The labile OM might represent carbohydrates (e.g. sugars) and lipids with a low humification degree, whereas the recalcitrant OM might represent aromatic compounds with a high humification degree (Barros *et al.*, 2011). The Fe(III)–HS system exhibited a first thermal event at temperatures >200°C, with a sharp dTGA peak at ~290°C (Table 3). The mass loss (~10.10%) was related to the decomposition of labile OM because previous studies indicated the difficulty of Fhy undergoing structural changes in this temperature range (Eggleton & Fitzpatrick, 1988). The temperature of the event at 550°C is compatible with the decomposition of recalcitrant OM. However, for Mnt–HS, there was virtually no mass loss in the temperature range of ~200–400°C, and the

https://doi.org/10.1180/clm.2023.30 Published online by Cambridge University Press

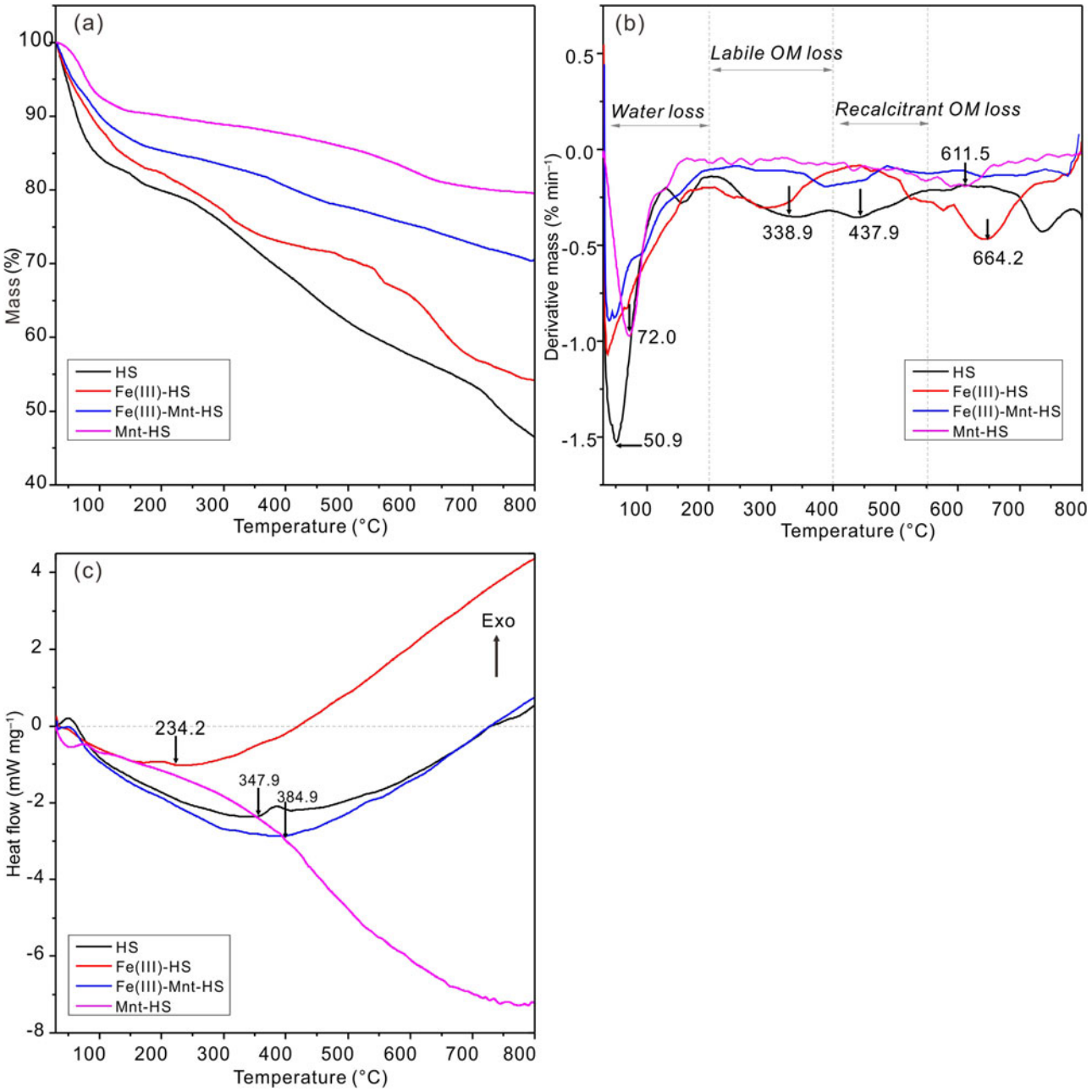

Figure 5. (a) TGA data of mass loss of HS and MOAs. (b) Derivative 'mass loss' of HS and MOAs. (c) DSC of HS and MOAs.

greatest mass loss mainly occurred at <200°C (Fig. 5b & Table 3). The thermal event at 612°C corresponds to the release of structural water (He *et al.*, 2005). Similarly, a peak at 387°C (i.e. <400°C) was recorded in the Fe(III)–Mnt–HS sample (Fig. 5b). This sample displayed a second step at 559°C. Compared to the HSs, the proportion of labile OM in the MOAs decreased by 6.3% for Fe(III)–HS and by 63.7% for Fe(III)–Mnt–HS (Table 3). The proportion of recalcitrant OM in the MOAs decreased by 59.4% for Fe(III)–HS and by 58.0% for Fe(III)–Mnt–HS. These results indicate that Fhy exhibited a tendency to combine with liable OM more frequently in the HS solutions. The hydroxyl (–OH) groups on mineral surfaces alongside the carboxyl and phenolic OH groups of the OM are critical for this combination reaction. Interestingly, the thermal analysis showed a peak at ~202°C with a mass loss of 3.36%. This mass loss may be due to the decomposition of some OM, which was catalysed by clay minerals (Bu *et al.*, 2017; Liu *et al.*, 2018).

Dehydroxylation is an endothermic process that is highlighted by negative peaks in the DSC data (Fig. 5c) at the same temperatures (i.e. ~280°C and ~480°C) with substantial mass loss. For the three samples (HS, Fe(III)–HS and Fe(III)–Mnt–HS), the endothermic peak temperatures were 347.9°C, 234.2°C and 384.9°C, respectively, and the energies were 2.36, 1.03 and 2.88 mW mg^{-1}, respectively. Accordingly, the temperature and energy required for the heat absorption decreased upon Fe(III) addition. However, the addition of Fe(III) and Mnt at same time resulted in increasing the temperature and energy required for heat absorption.

https://doi.org/10.1180/clm.2023.30 Published online by Cambridge University Press

Table 3. HS and thermal MOA attributes as functions of the clay.

Sample	SOC (%)[a]	dTGA (°C)	TG loss mass (%)	TG-T_{50}[b] (°C)	Exol/Exot[c]
HS	41.83	50.9	17.02	383.9	0.56
		100.9	3.02		
		338.9	10.78		
		437.9	9.62		
		736.9	13.13		
Fe(III)–HS	9.84	37.2	17.87	327.2	0.68
		290.2	10.10		
		550.2	3.91		
		644.2	13.89		
Mnt–HS	6.63	72.0	9.89	422.8	0.44
		611.5	4.11		
Fe(III)–Mnt–HS	5.17	39.9	14.48	390.9	0.54
		201.9	3.36		
		386.9	3.91		
		558.9	3.99		
		641.9	4.44		

[a]Total soil organic matter (SOC) is measured by C element analysis after acidification with hydrochloric acid.
[b]The temperature at which OM is half-decomposed.
[c]The proportion of thermally decomposed labile OM in the total OM.

OM thermal stability assessment

The thermal indices of OM stability were calculated based on the following data: (1) the temperature at which half of OM is decomposed (TG-T_{50}; Peltre *et al.*, 2013) and (2) the proportion of thermally decomposed labile OM in the total OM (Exol/Exot). A lower TG-T_{50} temperature promotes easier oxidation degradation for these organic compounds (Fernández *et al.*, 1997; Plante *et al.*, 2005; Rovira *et al.*, 2008). The HS, Fe(III)–Mnt–HS and Mnt–HS samples showed higher index TG-T_{50} values (384°C, 391°C and 423°C, respectively), whereas Fe(III)–HS showed a lower TG-T_{50} value (327.2°C; Table 3). The Exol/Exot ratios in the HS, Fe(III)–Mnt–HS, Mnt–HS and Fe(III)–HS samples were 0.56, 0.68, 0.44 and 0.54, respectively (Table 3). A higher Exol/Exot ratio was correlated with reduced OM stability. It is worth noting that Fhy can negatively influence the stability of HSs, whereas Mnt can improve the stability of HSs. Compared with Fe(III)–Mnt–HS, the degradation efficiencies of HSs alone and Fe(III)–HS were greater. Previous studies have shown that the oxidation-resistant fraction of mineral-associated OC was positively correlated with the Fe content and slightly negatively correlated with the clay content (Kirsten *et al.*, 2021).

Discussion

According to the findings in this study, the stability of the SOM is related to the interaction of Fe minerals and clay minerals. The fraction of C bonded with Mnt was effectively preserved, but the OM bonded with Fhy decomposed rapidly. This might be attributed to the differences in the soil mineral properties during SOM development. First, we considered the selectivity of minerals in SOM. The precipitation of HSs during Fhy co-precipitation in the MOAs induced the fractionation of organic compounds. The labile OM was preferentially adsorbed on the surface of Fhy. Parts of OM on the mineral surfaces may have initiated the catalytic process at lower temperatures, thus reducing the amount of energy required for OM breakdown and combustion. Similar phenomena have been observed in real soil systems worldwide (Faure *et al.*, 2006). Previous research on the pyrolysis behaviour of beech leaf litter in the presence of various soil minerals (i.e. Mnt and Fhy) showed that Fhy could promote the degradation of SOM (Miltner & Zech, 1997). CO_2 was released during the thermal decomposition of SOM in the presence of soil minerals under an N_2 atmosphere, and Fhy produced more CO_2 than Mnt (Miltner & Zech, 1997).

Second, the attachment of OM on mineral surfaces is typically dynamic and dependent on several factors, such as surface charge, surface topography and crystal structures (Kirsten *et al.*, 2021). In this work, temperature-dependent alteration in the Fe mineral phase was observed. During the pyrolysis of the MOAs under anaerobic conditions, the original amorphous Fhy was transformed into crystalline magnetite (Mgt; Fig. 6a). Mgt was generated at 300°C in the Fe(III)–Mnt–HS system, whereas in the Fe(III)–HS system it was produced at 200°C (Fig. 6c). The newly formed Fe mineral may lead to the creation of pores or defects, which might trigger the decomposition of OM. The Fe mineral phase changed, as was indicated by the FTIR spectrum of Fe(III)–HS, which showed the disappearance of the OH stretching vibration (~3352 cm^{-1}) for the heated samples (Fig. 6d & Table S2). The interlayer structure of Mnt had a considerable impact on the stability of Fe–OM complexes, as was evidenced by the higher d_{001} values of Fe(III)–Mnt–HS and the lower d_{001} values of Mnt–HS (Fig. 6b,c). These findings suggest that the interlayer OM is resistant to degradation at high temperatures because of Fe speciation.

In addition, new organic functional groups such as the amide II band (1554 cm^{-1}), symmetric of R–COO^- stretching (1381 cm^{-1}) and the amide III band (1267 cm^{-1}) emerged after a high-temperature anaerobic process was conducted (Fig. 6f & Table S2; Calderón *et al.*, 2013; Bu *et al.*, 2019; Meng *et al.*, 2022). At 200°C, 300°C and 400°C, these surface functional groups were almost invariant with ageing duration. Figure 6d shows a broad band at 3382 cm^{-1} that was attributed to the N–H stretching vibration and may indicate the presence of an amide A band (Ji *et al.*, 2020). For the Fe(III)–Mnt–HS system, the amide II band at 1547 cm^{-1} appeared at 200°C and 300°C and disappeared at 400°C (Fig. 6d). The amide II band most probably resulted from a C chain bond stretching vibration associated with the carbonyl group (C=O). The main source of the amide III band was methyl-related C–H or C–C stretching vibrations. The main source of the amide A band was the H–N stretching/bending vibration or the hydroxyl H–O stretching/bending vibration (Ji *et al.*, 2020).

Our data support the notion that soil mineralogical properties play a key role in determining the OC content of the soil. Particularly in systems where Fe(III) is present, the clay minerals contribute to the thermal stability of the SOM. This finding suggests that the soils comprising Fe(III)–aluminous clays exhibit greater OM persistency and are thus more resistant to disruptions induced by a high-temperature anaerobic process. The potential mechanism that could account for our experimental findings is as follows:

(1) In solution, co-precipitation of Mnt inhibited the formation of Fhy (the Fe fraction is reduced) and reduced the adsorption of labile OM. The interfacial reaction between Fe species and OM could have been altered by the presence of Mnt, which accounts for these observations. The co-precipitated HS might form a complex with Fe(III) mainly via carboxyl groups. Although Mnt would positively influence some OM adsorption and fractionation, it might also cause some OM to intercalate into the interlayer space of Mnt. In kaolinite–Fe(III)–malic acid systems, previous research proposed that

https://doi.org/10.1180/clm.2023.30 Published online by Cambridge University Press

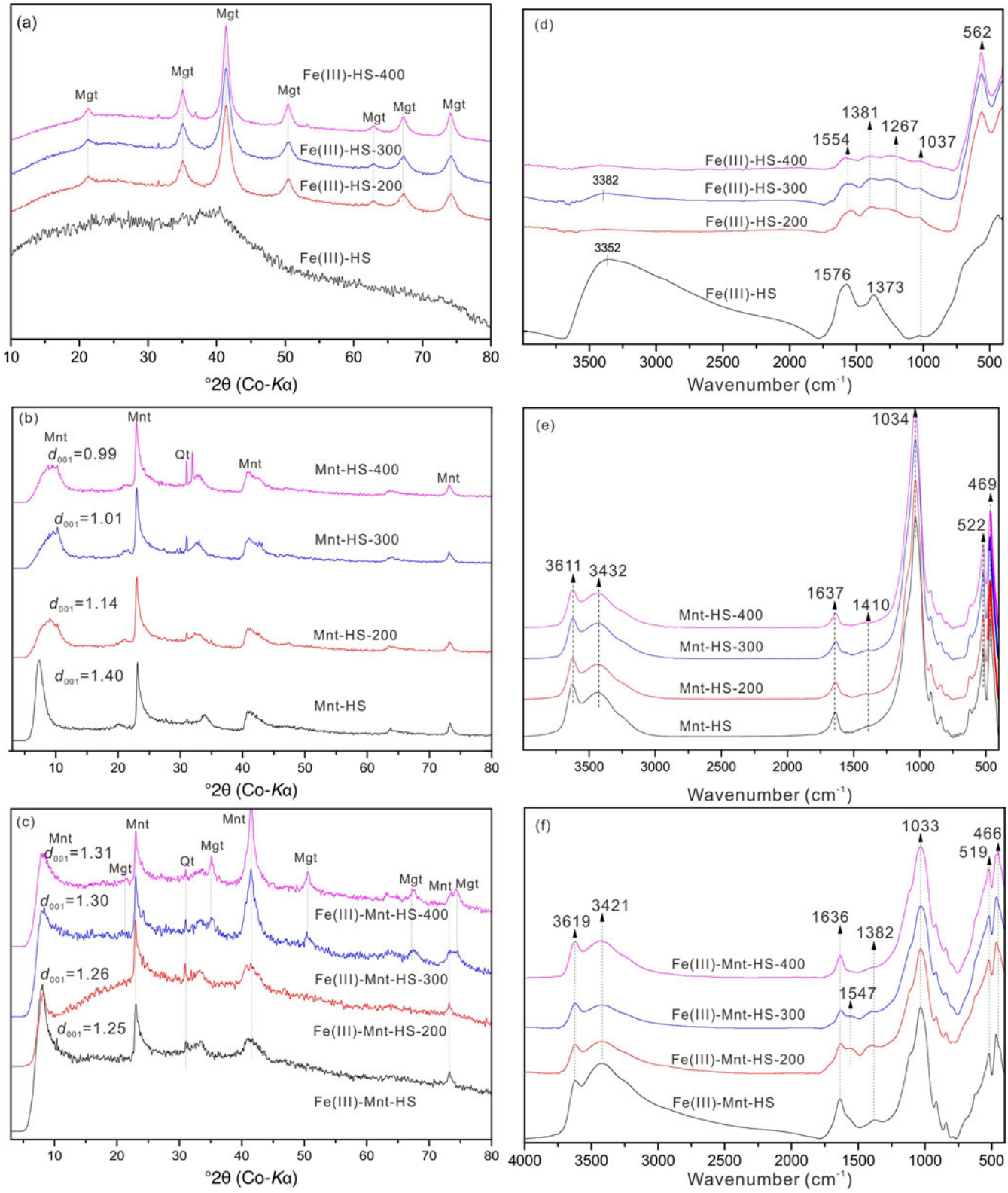

Figure 6. XRD traces of (a) Fe(III)–HS, (b) Mnt–HS and (c) Fe(III)–Mnt–HS before and after ageing. FTIR spectra of (d) Fe(III)–HS, (e) Mnt–HS and (f) Fe(III)–Mnt–HS before and after ageing. Mgt = magnetite; Qt = quartz.

Fe species might contribute to the complexation with OM via tetrahedral Fe bridges at smaller Fe/OM molar ratios, whereas the produced Fhy might induce adsorption and/or co-precipitation of OM molecules at greater Fe/OM molar ratios (Yang et al., 2017). This suggests that Mnt will selectively preserve OM in the soil solution in Fe(III)–Mnt–OM systems and emphasizes the role of Mnt in the Fhy-induced adsorption/co-precipitation of OM.

https://doi.org/10.1180/clm.2023.30 Published online by Cambridge University Press

(2) Labile OM on Fhy decomposes when the soil undergoes a high-temperature anaerobic heating process in a dry state. The transformation of Fhy occurs gradually. The dehydration, dehydroxylation and recrystallization of Fe (hydr)oxides could affect their surface physical chemical properties, which may cause some OM combined with Fe(III) to become unprotected and lead to inclusion, occlusion and entrance into the Fe (hydr)oxide crystal. Recalcitrant OM is a dominant component of Fe(III)–Mnt–HS. The Mnt disperses the Fhy particles and combines with some of them, thereby preventing a phase transition, further inhibiting the OM occlusion in Fhy. Previous studies demonstrated that Mnt influenced the mobility and fate of associated OM (Zhao et al., 2022) and inhibited the transformation of Fhy (Zhang et al., 2023). In addition, OM influenced the physiochemical properties of Fe oxide minerals, leading to more defects and porosity than in those formed from pure Fhy (Lu et al., 2019), which may create a greater area for the sequestration of OM. Accordingly, the clay minerals control the thermal behaviour of SOM via Fe (oxyhydr)oxides in terms of the aluminosilicate-induced reactions and their associations with Fe (oxyhydr)oxides in the soil.

The function of clay minerals in the actual soil system goes beyond this description. The interlayer space of expandable clay minerals might accommodate positively charged organics *via* cation exchange (Yuan *et al.*, 2013), which could affect the accommodation performance of these minerals for OM (Liu *et al.*, 2018). This finding is consistent with the widely acknowledged phenomenon that the amount of available inorganic surface area determines how long OM is preserved (Kögel-Knabner *et al.*, 2008; Kleber *et al.*, 2015). Numerous studies have indicated that the interlayer space of clay minerals hosts OM in soil and sediment samples (Schulten *et al.*, 1996; Lagaly *et al.*, 2006). The interlayer can stabilize OM against biological attacks as well as decomposition and mineralization processes. The results of this study indicate that expandable clay minerals in the soil should be studied further and could contribute more than other minerals to the stability of C in temperate-zone soils.

Conclusions

In this study, we used thermal analysis techniques to demonstrate the major impacts of Fe speciation on the stability of HSs in a ternary Fe(III)–Mnt–HS system. Given that Mnt particles were negatively charged and frequently combined with Fe (hydr)oxides in soils (Regelink *et al.*, 2014), ternary complexes of Fe between HSs, clays and Fhy should exist, which probably contributes to HS stability through Fhy-induced adsorption, co-precipitation or ternary complexation of HSs *via* Fe bridges on Mnt. During the co-precipitation of HSs, Mnt impacts the fractionation of HSs. Labile OM prefers to combine with Fe species. As Fhy cannot convert (i.e. it is suppressed) in the presence of Mnt, some labile OM has been retained and stabilized by the Fe species. Therefore, it is concluded that the speciation of Fe in the Fe(III)–clay–HS system controls the amount of C connected to minerals, particularly in the dry state. To fully understand how clay–OM interactions affect OM stability and C sequestration, further experiments involving a wider variety of relevant SOM, clay mineral species and environmental factors are required.

Acknowledgements. The authors thank LetPub (www.letpub.com) for linguistic assistance during the preparation of this manuscript.

Financial support. This work was financially supported by the Guangdong Academy of Sciences's Project of Science and Technology Development (no. 2020|GDASYL-20200102019, 2019GDASYL-0102002-5), Guangdong Basic and Applied Basic Research Foundation (2021A1515011540) and the National Natural Science Foundation of China (42107046).

Supplementary material. To view supplementary material for this article, please visit https://doi.org/10.1180/clm.2023.30.

References

Ahmat A.M., Thiebault T. & Guégan R. (2019) Phenolic acids interactions with clay minerals: a spotlight on the adsorption mechanisms of gallic acid onto montmorillonite. *Applied Clay Science*, **180**, 105188.

Bao Y., Bolan N.S., Lai J., Wang Y., Jin X., Kirkham M. *et al.* (2022) Interactions between organic matter and Fe (hydr)oxides and their influences on immobilization and remobilization of metal(loid)s: a review. *Critical Reviews in Environmental Science and Technology*, **52**, 4016–4037.

Barré P., Fernandez-Ugalde O., Virto I., Velde B. & Chenu C. (2014) Impact of phyllosilicate mineralogy on organic carbon stabilization in soils: incomplete knowledge and exciting prospects. *Geoderma*, **235**, 382–395.

Barreto M.S.C., Elzinga E.J., Ramlogan M., Rouff A.A. & Alleoni L.R.F. (2021) Calcium enhances adsorption and thermal stability of organic compounds on soil minerals. *Chemical Geology*, **559**, 119804.

Barros N., Cole J.J., Tranvik L.J., Prairie Y.T., Bastviken D., Huszar V.L. *et al.* (2011) Carbon emission from hydroelectric reservoirs linked to reservoir age and latitude. *Nature Geoscience*, **4**, 593–596.

Bosetto M., Arfaioli P., Pantani O. & Ristori G. (1997) Study of the humic-like compounds formed from L-tyrosine on homoionic clays. *Clay Minerals*, **32**, 341–349.

Bruun T.B., Elberling B. & Christensen B.T. (2010) Lability of soil organic carbon in tropical soils with different clay minerals. *Soil Biology and Biochemistry*, **42**, 888–895.

Bu H., Yuan P., Liu H., Liu D., Liu J., He H. *et al.* (2017) Effects of complexation between organic matter (OM) and clay mineral on OM pyrolysis. *Geochimica et Cosmochimica Acta*, **212**, 1–15.

Bu H., Yuan P., Liu H., Liu D., Qin Z., Zhong X. *et al.* (2019) Formation of macromolecules with peptide bonds *via* the thermal evolution of amino acids in the presence of montmorillonite: insight into prebiotic geochemistry on the early Earth. *Chemical Geology*, **510**, 72–83.

Calderón F., Haddix M., Conant R., Magrini-Bair K. & Paul E. (2013) Diffuse-reflectance Fourier-transform mid-infrared spectroscopy as a method of characterizing changes in soil organic matter. *Soil Science Society of America Journal*, **77**, 1591–1600.

Chen C., Dynes J.J., Wang J., Karunakaran C. & Sparks D.L. (2014) Soft X-ray spectromicroscopy study of mineral–organic matter associations in pasture soil clay fractions. *Environmental Science & Technology*, **48**, 6678–6686.

Cotrufo M.F. & Lavallee J.M. (2022) Soil organic matter formation, persistence, and functioning: a synthesis of current understanding to inform its conservation and regeneration. *Advances in Agronomy*, **172**, 1–66.

Demyan M., Rasche F., Schütt M., Smirnova N., Schulz E. & Cadisch G. (2013) Combining a coupled FTIR-EGA system and *in situ* drifts for studying soil organic matter in arable soils. *Biogeosciences*, **10**, 2897–2913.

Eggleton R.A. & Fitzpatrick R.W. (1988) New data and a revised structural model for ferrihydrite. *Clays and Clay Minerals*, **36**, 111–124.

Faure P., Jeanneau L. & Lannuzel F. (2006) Analysis of organic matter by flash pyrolysis–gas chromatography–mass spectrometry in the presence of Na-smectite: when clay minerals lead to identical molecular signature. *Organic Geochemistry*, **37**, 1900–1912.

Fernández I., Cabaneiro A. & Carballas T. (1997) Organic matter changes immediately after a wildfire in an Atlantic forest soil and comparison with laboratory soil heating. *Soil Biology and Biochemistry*, **29**, 1–11.

He H., Ding Z., Zhu J., Yuan P., Xi Y., Yang D.& Frost R.L. (2005) Thermal characterization of surfactant-modified montmorillonites. *Clays and Clay Minerals*, **53**, 287–293.

Hobbie S.E., Ogdahl M., Chorover J., Chadwick O.A., Oleksyn J., Zytkowiak R. & Reich P.B. (2007) Tree species effects on soil organic matter dynamics: the role of soil cation composition. *Ecosystems*, **10**, 999–1018.

Ji Y., Yang X., Ji Z., Zhu L., Ma N., Chen D. *et al.* (2020) DFT-calculated IR spectrum amide I, II, and III band contributions of *n*-methylacetamide fine components. *ACS Omega*, **5**, 8572–8578.

Karlsson T. & Persson P. (2012) Complexes with aquatic organic matter suppress hydrolysis and precipitation of Fe(III). *Chemical Geology*, **322**, 19–27.

Kirsten M., Mikutta R., Vogel C., Thompson A., Mueller C.W., Kimaro D.N. *et al.* (2021) Iron oxides and aluminous clays selectively control soil carbon storage and stability in the humid tropics. *Scientific Reports*, **11**, 5076.

Kleber M., Eusterhues K., Keiluweit M., Mikutta C., Mikutta R. & Nico P.S. (2015) Mineral–organic associations: formation, properties, and relevance in soil environments. *Advances in Agronomy*, **130**, 1–140.

Kögel-Knabner I., Guggenberger G., Kleber M., Kandeler E., Kalbitz K., Scheu S. *et al.* (2008) Organo-mineral associations in temperate soils: integrating biology, mineralogy, and organic matter chemistry. *Journal of Plant Nutrition and Soil Science*, **171**, 61–82.

Kopittke P.M., Dalal R.C., Hoeschen C., Li C., Menzies N.W. & Mueller C.W. (2020) Soil organic matter is stabilized by organo-mineral associations through two key processes: the role of the carbon to nitrogen ratio. *Geoderma*, **357**, 113974.

Kurganova I., Merino A., de Gerenyu V.L., Barros N., Kalinina O., Giani L. & Kuzyakov Y. (2019) Mechanisms of carbon sequestration and stabilization by restoration of arable soils after abandonment: a chronosequence study on phaeozems and chernozems. *Geoderma*, **354**, 113882.

Lagaly G., Ogawa M. & Dékány I. (2006) Clay mineral organic interactions. *Developments in Clay Science*, **1**, 309–377.

Liu H., Yuan P., Liu D., Bu H., Song H., Qin Z. & He H. (2018) Pyrolysis behaviors of organic matter (OM) with the same alkyl main chain but different functional groups in the presence of clay minerals. *Applied Clay Science*, **153**, 205–216.

Lopez-Capel E., Bol R. & Manning D. (2005) Application of simultaneous thermal analysis mass spectrometry and stable carbon isotope analysis in a carbon sequestration study. *Rapid Communications in Mass Spectrometry*, **19**, 3192–3198.

Lu Y., Hu S., Wang Z., Ding Y., Lu G., Lin Z. *et al.* (2019) Ferrihydrite transformation under the impact of humic acid and Pb: kinetics, nanoscale mechanisms, and implications for C and Pb dynamics. *Environmental Science: Nano*, **6**, 747–762.

Lützow M., Kögel-Knabner I., Ekschmitt K., Matzner E., Guggenberger G., Marschner B. & Flessa H. (2006) Stabilization of organic matter in temperate soils: mechanisms and their relevance under different soil conditions – a review. *European Journal of Soil Science*, **57**, 426–445.

Meng F., Bu H., Fei Y., Chen M., Lei Q., Liu D. *et al.* (2022) Effects of clay minerals on Fe^{2+}-induced phase transformation of ferrihydrite. *Applied Geochemistry*, **144**, 105401.

Merino E. & Nevado C. (2014) Addition of CF_3 across unsaturated moieties: a powerful functionalization tool. *Chemical Society Reviews*, **43**, 6598–6608.

Mikutta R., Kleber M., Torn M.S. & Jahn R. (2006) Stabilization of soil organic matter: association with minerals or chemical recalcitrance? *Biogeochemistry*, **77**, 25–56.

Miltner A. & Zech W. (1997) Effects of minerals on the transformation of organic matter during simulated fire-induced pyrolysis. *Organic Geochemistry*, **26**, 175–182.

Muneer M., & Oades J.M. (1989) The role of Ca–organic interactions in soil aggregate stability. III. Mechanisms and models. *Soil Research*, **27**, 411–423.

Parfitt R., Theng B., Whitton J. & Shepherd T. (1997) Effects of clay minerals and land use on organic matter pools. *Geoderma*, **75**, 1–12.

Paul E.A. (2016). The nature and dynamics of soil organic matter: plant inputs, microbial transformations, and organic matter stabilization. *Soil Biology and Biochemistry*, **98**, 109–126.

Peltre C., Fernández J.M., Craine J.M. & Plante A.F. (2013) Relationships between biological and thermal indices of soil organic matter stability differ with soil organic carbon level. *Soil Science Society of America Journal*, **77**, 2020–2028.

Plante A., Pernes M. & Chenu C. (2005) Changes in clay-associated organic matter quality in a C depletion sequence as measured by differential thermal analyses. *Geoderma*, **129**, 186–199.

Regelink I.C., Voegelin A., Weng L., Koopmans G.F. & Comans R.N. (2014) Characterization of colloidal Fe from soils using field-flow fractionation and Fe K-edge X-ray absorption spectroscopy. *Environmental Science & Technology*, **48**, 4307–4316.

Rosell R.A., Andriulo A.E., Schnitzer M., Crespo M.B. & Miglierina A.M. (1989) Humic acids properties of an Argiudoll soil under two tillage systems. *Science of the Total Environment*, **81**, 391–400.

Rovira P., Kurz-Besson C., Coûteaux M.-M. & Vallejo V.R. (2008) Changes in litter properties during decomposition: a study by differential thermogravimetry and scanning calorimetry. *Soil Biology and Biochemistry*, **40**, 172–185.

Schnitzer M. & Monreal C.M. (2011) *Quo vadis* soil organic matter research? A biological link to the chemistry of humification. *Advances in Agronomy*, **113**, 139–213.

Schulten H.-R., Leinweber P. & Theng B. (1996) Characterization of organic matter in an interlayer clay–organic complex from soil by pyrolysis methylation–mass spectrometry. *Geoderma*, **69**, 105–118.

Schwertmann U. & Cornell R.M. (2008) *Iron Oxides in the Laboratory: Preparation and Characterization*. John Wiley & Sons, Hoboken, NJ, USA, 188 pp.

Sodano M., Lerda C., Nisticò R., Martin M., Magnacca G., Celi L. & Said-Pullicino D. (2017) Dissolved organic carbon retention by coprecipitation during the oxidation of ferrous iron. *Geoderma*, **307**, 19–29.

Sutton R. & Sposito G. (2006) Molecular simulation of humic substance–Ca-montmorillonite complexes. *Geochimica et Cosmochimica Acta*, **70**, 3566–3581.

Tokarski D., Wiesmeier M., Weissmannová H.D., Kalbitz K., Demyan M.S., Kučerík J. & Siewert C. (2020) Linking thermogravimetric data with soil organic carbon fractions. *Geoderma*, **362**, 114124.

Tombácz E., Libor Z., Illés E., Majzik A. & Klumpp E. (2004) The role of reactive surface sites and complexation by humic acids in the interaction of clay mineral and iron oxide particles. *Organic Geochemistry*, **35**, 257–267.

Wattel-Koekkoek E.J.W., Van Genuchten P.P.L., Buurman P. & Van Lagen B. (2001) Amount and composition of clay-associated soil organic matter in a range of kaolinitic and smectitic soils. *Geoderma*, **99**, 27–49.

Yang J., Liu J., Hu Y., Rumpel C., Bolan N. & Sparks D. (2017) Molecular-level understanding of malic acid retention mechanisms in ternary kaolinite–Fe(III)–malic acid systems: the importance of Fe speciation. *Chemical Geology*, **464**, 69–75.

Ye G., Deng H., Zhou S., Gao Y. & Yan C. (2022) Coupling humic acid in Fe-bearing montmorillonite for enhanced adsorption and catalytic degradation of tetracycline. *Environmental Science and Pollution Research*, **29**, 90984–90994.

Ye Z., Padilla J.A., Xuriguera E., Brillas E. & Sirés I. (2020) Magnetic MIL (Fe)-type MOF-derived N-doped nano-ZVI@C rods as heterogeneous catalyst for the electro-Fenton degradation of gemfibrozil in a complex aqueous matrix. *Applied Catalysis B: Environmental*, **266**, 118604.

Yuan L., Lin W., Zheng K., He L. & Huang W. (2013) Far-red to near infrared analyte-responsive fluorescent probes based on organic fluorophore platforms for fluorescence imaging. *Chemical Society Reviews*, **42**, 622–661.

Zeng Q., Huang L., Ma J., Zhu Z., He C., Shi Q. *et al.* (2020) Bio-reduction of ferrihydrite–montmorillonite–organic matter complexes: effect of montmorillonite and fate of organic matter. *Geochimica et Cosmochimica Acta*, **276**, 327–344.

Zhang T., Tang B. & Fu F. (2023) Influence of montmorillonite incorporation on ferrihydrite transformation and Cr(VI) behaviors during ferrihydrite–Cr(VI) coprecipitates aging. *Science of the Total Environment*, **873**, 162257.

Zhao Y., Moore O.W., Xiao K.-Q., Curti L., Fariña A.O., Banwart S.A. & Peacock C.L. (2022) The role and fate of organic carbon during aging of ferrihydrite. *Geochimica et Cosmochimica Acta*, **335**, 339–355.

https://doi.org/10.1180/clm.2023.30 Published online by Cambridge University Press